Graphene Oxide as an Efficient Antimicrobial

Nanomaterial for Eradicating Multi-Drug Resistant

Bacteria in Vitro and in Vivo

Xu Wu <sup>1</sup>, Shirui Tan <sup>2</sup>, Yuqian Xing, <sup>1</sup> Qinqin Pu <sup>2</sup>, Min Wu <sup>2,\*</sup>, Julia Xiaojun Zhao <sup>1,\*</sup>

KEYWORDS: Graphene oxide, antimicrobial, *Klebsiella pneumoniae* (*Kp*), infectious diseases.

Abstract.

Graphene is a novel two-dimensional nanomaterial with a growing number of practical

applications across numerous fields. In this work, we explored potential biomedical applications

of graphene oxide (GO) by systematically studying antibacterial capacity of GO in both

macrophages and animal models. Three types of bacteria, including Klebsiella pneumoniae (Kp),

Escherichia coli (E. coli) and P. aeruginosa (Pa) were used for in vitro study. Kp was also selected

as a representative multidrug resistant (MDR) bacterium for in vivo study.

In in vitro study, GO effectively eradicated Kp in agar dishes and thus protected alveolar

macrophages (AM) from Kp infection in the culture. In the in vivo evaluation, GO were introduced

intranasally into mouse lungs followed by testing, organ tissue damage including lung, liver,

1

spleen, and kidneys, polymorphonuclear neutrophil (PMN) penetration, bacterial dissemination, and mortality in *Kp*-infected mice. We found that GO can contain and eradicate the growth and spread of *Kp* both *in vitro* and *in vivo*, resulting in significantly increased cell survival rate, less tissue injury, subdued inflammatory response, and prolonged mice survival. These findings indicate that GO could be a promising biomaterial for effectively controlling MDR pathogens.

### 1. Introduction.

Multi-drug resistant superbugs are becoming alarmingly common in recent years and are currently a serious global health issue. Excessive and improper usage of antibiotics in past decades played a major role in this problem. For instance, Klebsiella pneumoniae (Kp), a clinically significant pathogen, continuously acquires carbapenem-resistant properties due to wide applications of carbon penicillin antibiotics in hospitals.[1, 2] Further, Kp can easily infect patients who have pre-existing conditions such as cystic fibrosis, asthma and emphysema.[2] Therefore, development of new effective antibiotics and/or therapeutic agents is crucial for fighting against multiple-drug-resistant (MDR) bacteria.[3] In recent years, the rapid advancement of nanoscience and nanotechnology has produced several antibacterial nanomaterials.[4-6] The antibacterial mechanisms of these nanomaterials are not well understood but may be different from those of conventional antibiotics, which suggests that the nanomaterials could be used as complementary or alternative agents for treating MDR bacterial infection.[7, 8] For example, silver nanoparticles have been reported for effectively eradicating bacteria with size and shape dependence.[8-10] More recently, graphene, a new 2-dimensional carbon nanomaterial, has shown great potential as an antibacterial agent.[11-15]

Graphene has been tested for a variety of applications owing to its large surface area to volume ratio and excellent mechanical, electric, and optical properties.[16, 17] Among these applications, the biomedical potential of graphene-based nanomaterials is a recent development and has attracted researchers' attentions. So far, graphene-derivatives, including graphene oxide (GO), reduced graphene oxide (RGO), graphene quantum dots (GQDs) and graphene-based nanocomposites, have been applied to biosensors, [18, 19] bioimaging, [20-22] drug delivery, [23, 24] and photothermal therapy. [25-27] Moreover, graphene-derivatives were found to have in vitro antibacterial properties. Graphene oxide and reduced graphene oxide exhibited toxicity to both Gram-positive and Gram-negative bacteria.[11, 12] Liu et al. compared the antibacterial properties of four different carbon materials, including graphite, graphite oxide, GO and RGO.[28] They found that GO possessed the highest antibacterial activity while graphite oxide exhibited the lowest antibacterial capacity. Meanwhile, they proposed a three-step antimicrobial mechanism for graphene-based nanomaterials antibacterial activity, including cell deposition on graphene nanomaterials, membrane disruption by sharp nanosheets, and superoxide anion-independent oxidation. The lateral size of GO affected their antibacterial activity. [29] Larger GO sheets also resulted in stronger antibacterial activity than smaller ones because the larger GO sheets could effectively isolate bacterial cells from surroundings by wrapping the entire cell wall of the bacterium.[30, 31] Three main possible antimicrobial mechanisms of graphene nanomaterials have been proposed: i) inducing cellular trauma with sharp edges of the nanomaterial; ii) oxidative stress caused by the generation of superoxides with treatment of graphene nanomaterials; and iii) wrapping or trapping the bacteria, and limiting physical movements and metabolism of bacteria. In another example, Mangadlao et al reported that the edges of GO were not the fundamental part of the mechanism of its antibacterial activity.[32] Even though it is unclear which of the proposed

mechanism is central to graphene nanomaterials' antibacterial properties, their efficacy is well observed and recognized.[33, 34] However, most of these studies only demonstrated antibacterial activity in common *in vitro model* bacteria such as *Escherichia coli* (*E. coli*) and *Staphylococcus aureus* (*Sa*). To further understand whether or not the graphene nanomaterials is an antimicrobial biomaterial in a wider range of experimental and real world conditions, evaluation of the graphene nanomaterials in mammalian cells and animals models in the presence of MDR bacteria would yield additional insight to antimicrobial property of graphene nanomaterials. Additionally, *in vivo models* would also provide an opportunity to study potential toxicity of graphene based nanomaterial

In this study, we have addressed these questions by systematically investigating the infectious ability of MDR bacteria in the presence of graphene nanomaterials both *in vitro* and *in vivo*. Kp was selected as a representative MDR bacterium for this study because it is the most common pathogens in nosocomial infections. After treatment using GO, the invasive potency of Kp was explored in both macrophages and mouse models. The results showed that GO could effectively inhibit Kp growth in a concentration dependent manner. The infectious ability of Kp was dramatically inhibited in both macrophages and mice after GO treatment.

# 2. Methods and Materials.

**2.1 Materials and Instruments.** Female C57BL/6J mice of 8 week-olds were purchased from Charles River (San Diego, CA). *Klebsiella pneumonia* (*Kp*) Xen-39 (ATCC 93A 5370), a bioluminescent pathogenic bacterium strain expressing LUC bioluminescence was purchased from Caliper (Santa Clara, CA). *Kp* (ATCC 43816 serotype II) was obtained from Dr. Virginia Miller (University of North Carolina). *Kp* Xen-39 (ATCC 43816) was used for the bioluminescence

imaging experiment and *Kp* (ATCC 43816 serotype II) was used for other infection of mice. *Pseudomonas aeruginosa* (Pa) WT PAO1 was a gift from S. Lory (Harvard Medical School, Boston, MA). *E. coli* HB101 strain and mouse alveolar macrophage cell line (MH-S) were obtained from American Tissue Culture Collection (ATCC). All of the animal experiments were approved by Institutional Animal Care and Use Committee (IACUC) in the University of North Dakota. Graphene oxide (GO) was purchased from Cheap Tubes Inc. (Grafton, VT). Phosphate buffered saline tablets and fetal bovine serum were purchased from Fisher Scientific (Waltham, MA). Deionized (DI) water (Millipore Milli-Q grade) with resistivity of 18.2 MΩ•cm was used in all experiments.

A Hitachi SU8010 field emission scanning electron microscope (SEM) was used to capture SEM and STEM images of GO. A Zetasizer (Marlwen, model of Nano-ZS, Westborough, MA) was used to measure Zeta potentials of GO. UV-vis absorption spectra were recorded with a Lambda 1050 UV/VIS/NIR spectrometer (PerkinElmer, Santa Clara, CA). Luminescence images were taken using a Caliper's Xenogen IVIS optical imaging system (Caliper, PerkinElmer, Santa Clara, CA). The OD values at 560 nm for 3-(4,5-dimethyl-2-thiazolyl)-2,5- diphenyltetrazolium bromide (MTT) and nitroblue tetrazolium (NBT) assays were measured using a multissan spectrum spectrophotometer (Thermofisher Scientific, Waltham, MA).

2.2 Analysis of Antibacterial Activity. *Kp* Xen-39 was cultured in Lysogeny broth (LB) medium with continuous shaking at 37 °C overnight.[35] The bacteria were harvested by centrifugation and dispersed in PBS with an optical density of 0.1 for a concentration of 10<sup>8</sup> CFU mL<sup>-1</sup> at 600 nm (OD<sub>600</sub>).[36] The GO samples in PBS were incubated with bacteria suspension for 2 h at 37 °C. An aliquot of 100 μL of bacteria suspension was added into 900 μL of LB medium for growth in a shaking incubator at 37 °C overnight. The concentration of bacteria was determined

by measuring  $OD_{600}$ . The bioluminescence images were taken using the IVIS optical imaging system. Meanwhile, the plate count method was used to demonstrate the bacteria killing effect of GO. Briefly, the bacteria suspension in LB medium treated with GO was plated on LB-agar plates and then incubated at 37 °C overnight. The antibacterial activity of GO to *E. coli* and *Pa* was investigated similarly as Kp.

**2.3 Bacteria Infection of Mammalian Cells.** The log-phase Kp bacteria (OD<sub>600</sub> = 1.0) were incubated with different concentrations of GO (Kp-GO) for 2 h in PBS buffer at 37 °C. The same Kp bacteria without treatment of GO were used as a control. An aliquot of 0.1 mL of Kp-GO and control Kp bacteria were both diluted with 0.9 mL of LB medium for incubation at 37 °C overnight. Then, murine alveolar macrophage (MH-S) cells were infected with control Kp and Kp-GO for 8 h. MH-S cells were infected by Kp at multiplicity of infection (MOI) 10:1 (bacteria-cell ratio) and then washed three times with PBS to remove floating bacteria. Bacteria on the cell surface were killed by adding 100  $\mu$ L of polymyxin B and left in incubation for another 1 h. The viability of MH-S cells after infection was determined by MTT assay.[37] Briefly, 1  $\mu$ g/mL MTT (in 10  $\mu$ l) was added into each well and incubated at 37°C until color change.[38] MTT was reduced to form a purple formazan product inside living cells. Afterward, a stop solution was added to dissolve the formazan product, and the solution absorbance was quantified at 560 nm using a spectrometer plate reader.[39]

**2.4 Analysis of Bacteria Infection in Mice.** First, the Kp bacteria (OD<sub>600</sub> =0.1) were treated with 0.25 mg/mL GO (Kp-GO) for 2 h in PBS buffer at 37 °C. The Kp bacteria without treatment of GO were used as a control. Then, the Kp bacteria and Kp-GO bacteria were diluted to  $2 \times 10^6$  CFU/mL for further experiments. For *in vivo* imaging of the bioluminescent Kp Xen-39 in mice, an aliquot of 50  $\mu$ L of Kp and Kp-GO were intraperitoneally injected into two groups of mice after

anesthesia with 40 mg/kg ketamine. The bioluminescence images were taken under the IVIS optical imaging system at varying time periods from 0 to 24 h. The infection level was semiquantitively evaluated using the bioluminescence intensity determined by ROI calculation using the IVIS software.[35]

For further analysis of the antibacterial efficiency of GO *in vivo*, the mice anesthetized with 40 mg/kg ketamine were instilled with *Kp* and *Kp*-GO by intranasal instillation, and sacrificed when they were moribund. Survivals were determined using Kaplan–Meier curves. After bronchoalveolar lavage (BAL), the lung was excised for homogenization and fixed in 10% formalin for histological analysis. The formalin-fixed lung tissue was used for H&E staining to examine tissue damage post infection.

The viability of alveolar macrophages (AM) was evaluated using MTT assay. Briefly, the AM cells were obtained from mice infected with *Kp* and *Kp*-GO. The AM cells in each well were mixed with 1 μg/mL MTT and incubated at 37°C until color change as dscribed above.[40] The superoxide anion in AM cell after infection was measured using NBT assay. AM cells were grown in serum-containing medium at 37°C for 4 h and then mixed with 1 μg/mL NBT dye for another 1 h. An aliquot of 100 μL of stop solution (10% DMSO; 10% SDS in 50 mM HEPES buffer) was added into each well to terminate the reaction. The absorbance at 560 nm was measured using the plate reader after overnight incubation at 37°C.[41]

To evaluate the infection severity of *Kp*-GO in mice, the alive *Kp* amounts in several organs, including lung, liver, kidneys and spleen were analyzed. The organs were obtained from different mice groups at varying time points. Then, the organs were obtained to determine the amounts of intracellular bacteria through CFU. Briefly, the tissues were homogenized with PBS and spread

on LB plates to enumerate level of bacteria. The plates were cultured in a 37°C incubator overnight, and colonies were counted. Meanwhile, the amounts of myeloperoxidase (MPO) released from the four different organs were analyzed using MPO assay. Briefly, the 100 mg/mL tissue samples were homogenized in 50 mM hexadecyltrimethylammonium bromide, 50 mM KH<sub>2</sub>PO<sub>4</sub>, pH 6.0, 0.5 mM EDTA and centrifuged for 15 min at 12,000 rpm at 4°C. Supernatants were decanted, and 100 μL of reaction buffer (0.167 mg/mL O-dianisidine, 50 mM KH<sub>2</sub>PO<sub>4</sub>, pH 6.0, 0.0005% mM H<sub>2</sub>O<sub>2</sub>) were added to 100 μL of sample. After 2 min, the absorbance was measured at 460 nm using a spectrometer plate reader.

- **2.5 Statistical Analysis.** All experiments were performed in triplicates and for three times. Data were shown as mean  $\pm$  SE (standard error) from the three independent experiments. All error bars stand for SE. Group means were compared using Student's *t*-test or one-way ANOVA, using Graphpad Prism 5 software (La Jolla, CA).
- 2.6. Preparation of GO. The commercial available GO were dispersed into water through ultrasonic to obtain stable GO solution. Briefly, 40 mg NaOH was added to an aliquot of 100 mL of 50 μg/mL GO. NaOH could increase the zeta potential of GO because it would form COO- and O- groups on the surface of GO, and thus increase the GO stability. The solution was placed in an ultrasonic bath for 3 h to form a stable GO solution. Afterwards, large aggregates were removed by centrifuging at 8,000 rpm for 10 min and the supernatant was remained. The pH of the final GO solution was adjusted to 7.00 in PBS buffer for following biological applications.

## 3. Results and Discussion.

**3.1 Characterization of GO.** The GO solution was prepared as described in section 2.6. Several characterization experiments were conducted to confirm the GO morphology and

composition prior to bioapplications. First, the morphology of GO was characterized using scanning transmission electron microscopy (STEM). As shown in Figure 1A, the size of GO sheet is in the range of micrometers. Wrinkles and folds were clearly observed on the STEM image, indicating the single layers and flexibility of the GO sheets. Afterwards, an elemental analysis of GO was conducted using Energy-dispersive X-ray spectroscopy (EDS) (Figure 1B). The EDS result clearly showed the presence of carbon and oxygen. To further confirm that the oxygen was present as surface groups of GO, zeta potentials of GO was measured as shown in Figure 1C. The peak value of -45 mV showed the presence of negatively charged oxygen, indicating that they are on the surface of GO. The high level of negative charge ensured the stability of GO solution. Finally, UV-vis absorption spectrum was measured to characterize the GO absorption peak. As shown in Figure 1D, a strong peak at ca. 230 nm was due to the  $\pi$ -plasmon of  $sp^2$  carbon structure and the shoulder around 300 nm was ascribed to the n to  $\pi^*$  transitions. The above characterizations confirmed the GO composition and morphology.

3.2 Antibacterial Property of GO at Bacteria Levels. The antibacterial activity of GO was initially investigated at bacterial level prior to *in vivo* study. Three types of bacteria were used in this work, including MDR Gram-negative superbugs Kp, E. coli and P. aeruginosa (Pa). Due to the great need for anti-MDR bacteria materials, we first investigated the GO antibacterial property on Kp. Various GO concentrations were used ranging from 0 to 500.0  $\mu$ g/mL. After incubation of the GO with bacterial cells as described in section 2.2, the OD600 values of each solution were detected to measure the bacteria survival rate (Figure 2A). The Kp survival rate decreased from 100% to 28.8%, 15.2%, 2.8% and 3.2% when the concentrations of GO increased from 0 to 62.5, 125.0, 250.0 and 500.0  $\mu$ g/mL, respectively. In parallel, bioluminescence intensities of the bacterial solution were determined to further evaluate the bacteria eradication efficiency of GO

because the Kp strain can emit bioluminescence. As shown in the inset of Figure 2A, the bioluminescence intensity of Kp in LB medium decreased with increasing GO concentrations. The Kp survival rate is proportional to the bioluminescence intensities. These results indicated that the antibacterial activity of GO is concentration-dependent.

To qualitatively validate the results from the bioluminescence imaging and  $OD_{600}$  values, we further conducted bacterial colony forming unit (CFU) assay on LB-agar dishes (Figure 2B). The same amount of GO-treated Kp (Figure 2B a) and untreated Kp (Figure 2B b) were cultured overnight. In comparison of Figure 2B a and b (bright-field photographs), the amounts of bacterial colonies drastically decreased after GO treatment. Afterwards, their bioluminescence images of the same plates were taken (Figure 2B c and d). The GO treated Kp showed few bioluminescence spots while untreated Kp presented significant bioluminescence signals. Collectively, GO exhibited clear effectiveness of antibacterial activity to MDR superbug, Kp, at the bacterial level.

To evaluate whether the antibacterial activity of GO is ubiquitous, we then investigated another two Gram-negative bacteria, E. coli and P. aeruginosa (Pa) using the similar experiments as descried above for Kp. As shown in Figure 2C and D, GO has exhibited a comparable antibacterial activity with Kp to E. coli and Pa. Similar to the Kp data, with increasing the concentrations of GO, the survival rate of E. coli and Pa significantly decreased. The survival rate of E. coli and Pa were reduced to 11.8 % and 11.9 % when treated with 250  $\mu$ g/mL of GO (Figure 2C and D). Considering the importance of MDR bacteria, in the following  $in\ vitro$  and  $in\ vivo$  studies, Kp was chosen as a representative bacterium to investigate the GO antibacterial activity.

**3.3 Infectious Ability of** *Kp***-GO** *in vitro***.** After the *Kp* bacterial cells were treated with GO as described in section 2.3, the invasion ability or virulence of *Kp* was investigated in macrophage

(MH-S) cells, allowing 8 h of interaction of MH-S cells with the bacterial solution. The MH-S cells without any bacterial infection were used as a negative control. Varying concentrations of GO from 0 to 500.0 μg/mL were used. The MTT assay results were shown in Figure 3A. The cell viability increased with increasing GO concentration and reached a plateau of 65% at 250.0 μg/mL of GO. The result indicated that GO could kill *Kp* bacteria to certain extent in a concentration dependent manner.

To measure the intrinsic toxicity of GO on MH-S cells, the cytotoxicity of GO to cells was hence investigated under the similar conditions of Figure 3A. In Figure 3A when macrophages were infected, the final GO concentration was diluted by 10 times due to addition of culture medium. For instance, the concentration of 500  $\mu$ g/mL (pure) GO in Figure 3A equals a final concentration of 50  $\mu$ g/mL in Figure 3B. In order to be comparable with these concentrations, three GO concentrations including 5, 50 and 100  $\mu$ g/mL were selected to treat macrophages. Even with the highest concentration of 100  $\mu$ g/mL, the MH-S cell viability only decreased to *ca.* 90% (Figure 3B), indicating good biocompatibility of GO to cells. Therefore, we could reasonably exclude the impact of GO on cell viability during our analysis. It is reasonable to speculate that the significant difference between normal cells and *Kp*-GO treated cells (Figure 3A) is due to the strong infectious ability of a little remained alive *Kp*. The above results clearly demonstrated GO's antibacterial property *in vitro*. In order to further understand whether or not GO could be a potential antibacterial reagent in physiological environments, *in vivo* investigation of GO treated *Kp* (*Kp*-GO) is needed.

**3.4 Infectious Ability of** *Kp***-GO** *in vivo***.** So far, the antibacterial activity of GO in animal models has not been explored. Using a mouse model, we investigated the effect of GO on the infection potency of *Kp in vivo*. To this end, we intraperitoneally injected GO-treated *Kp* into mice

at the concentration of  $1 \times 10^5$  CFU (in 50 µL PBS buffer) per mouse. Then, the bioluminescence imaging was carried out using the IVIS Lumina XRII system to monitor the invasion and dissemination of Kp in mice. As a control, mice injected with untreated Kp was first imaged as shown in Figure 4A (top). The images clearly showed diffusion and intense bioluminescence, indicating severe Kp infection. While bioluminescence stayed in the enterocoelia cavity in the early time period of Kp injection, it extended to the thoracic cavity at 8 h post injection. However, the dissemination areas and intensity of bioluminescence in mice infected by GO-treated Kp (250.0 µg/mL of GO) were more constrained as shown in Figure 4A (bottom). Even after 24 h post injection, the translocation of Kp to thoracic cavity was limited with GO-treated Kp. Then, we measured the bioluminescence intensity in these two groups (Figure 4B). The bioluminescence intensity of control Kp-infected mice was almost twice higher (1.6 - 2.0) than that of the mice infected by GO-treated Kp. This proved that the invasion ability of Kp could be inhibited by GO in mice.

Since Kp is a common cause of respiratory infection, we intranasally instilled Kp into mice lungs to investigate whether GO could impact the infection potency in the respiratory organs. As shown in Figure 5A, 50% of mice died within 48 h after the injection of untreated Kp, and of the remaining mice died within 72 h. In contrast, as high as 80% of mice infected by GO-treated Kp remained alive during the entire period of 72 h. The results demonstrated that GO could greatly inhibit the infection potency of Kp, decrease the mortality and prolong survival time of infected-mice.

After infection *via* intranasal instillation of *Kp*, the damage of the lung tissue was also examined using H&E staining. As shown in Figure 5B, the morphology of lung tissue was altered (Figure 5 B, middle) compared to the normal lung tissue (Figure 5 B, left), including signs of

inflammatory response, tissue damage, and severe pneumonia in the mice treated by untreated *Kp*. However, GO-treated *Kp* caused subdued inflammatory features, reduced polymorphonuclear neutrophil (PMN) penetration and decreased tissue damage (Figure 5 B, right). Therefore, GO can significantly alleviate the damage of lung tissue by reducing *Kp* infection ability.

To further delve into the antibacterial mechanism of GO *in vivo*, the viability of primary alveolar macrophages (AM) isolated from the infected mice was evaluated because AMs are key innate immunity cells in fighting against Gram-negative bacterial infection, particularly by phagocytizing and eradicating pathogens. The viability of AM reflects the cellular health state following bacterial infection. As shown in Figure 6A, the viability of AM from *Kp*-GO infected mice increased by approximately 1.4- and 3.1-fold compared to that of the untreated-*Kp* group at 24 h and 48 h post infection, respectively.

Meanwhile, the phagocyte-derived reactive oxygen species (ROS) is considered an important factor for eradicating the invading bacteria and indirect measurement of severity of infection. Severe infection will lead to excessive generation of ROS species (Figure 6B). At 8 h and 24 h post injection, GO-treatment significantly decreased the generation of ROS in AM, indicating reduction in infection extent. Furthermore, the quantity of PMN in BAL and blood of the infected mice was also measured to gauge inflammatory responses. As shown in Figure 6C and 6D, PMN penetration in both BAL fluid and blood of *Kp*-GO group was lower than that of *Kp* group at 8 h and 24 h post infection. Collectively, the overall data of AM cell viability, ROS species, and PMN penetration indicated that the infection potency of *Kp* was greatly dampened *in vivo* by GO treatment compared to the controls.

Another mortiferous factor for bacterial infection is spread to various organs during sepsis. Septicemia and ultimately sepsis might be caused by bacterial dissemination during disease progression. Therefore, we investigated Kp dissemination after intranasal instillation by determining bacterial burdens in the organs of lung, liver, spleen, and kidneys. As shown in Figure 7, the lung (A) showed the highest bacterial loads, followed by the spleen (C), kidney (D) and liver (B). However, in the all organs, bacterial CFUs from the mice infected with Kp-GO were significantly lower than those from the control group (untreated Kp) at 8 h and 24 h post infection. To validate this observation, we detected the activity of tissue injury, MPO, in all the organs as MPO is released from PMN in response to pulmonary infections. As shown in Figure 8, in the four organs, the activity of MPO followed the same trend as that of the bacterial CFUs in Figure 7. At 8 h and 24 h post infection, the MPO activity of GO-treated Kp group was significantly lower than that from sham-treated Kp group, indicating that GO treatment dramatically alleviated infection in mice.

By investigating the infection severity, survival rate, AM cell viability, ROS production and bacterial dissemination in mice after intranasally instilling Kp-GO and Kp, we found that the treatment of GO could significantly inhibit Kp growth and eliminate infection. However, even 250.0  $\mu$ g/mL of GO could inhibit 97.2 % proliferation of Kp in vitro (Figure 2A), infection still occurred when this Kp-GO was applied in mice, leading to 20% of treated mice's death. The treatment of GO with Kp could greatly prolong the survival time of the infected mice, alleviate the damage of lung tissue, and inhibit the dissemination in other organs after instillation. Despite significant improvement in disease and alleviation of injury, all the infectious parameters investigated suggest that GO treatment may not completely prevent infection from occurring (Figure 4-8). In other words, these results indicated that the antimicrobial activity investigation of

graphene materials in the bacterial level or in mammalian culture may not accurately predict the possible results when they were used *in vivo*. Further investigation regarding the antimicrobial activity of graphene materials should be conducted in animals before their translation into clinics.

### 4. Conclusions.

In conclusion, the antibacterial activity of GO to Kp was investigated at the bacterial, mammalian cell and animal levels in this work. At the bacterial level, GO can eradicate Kp in a concentration-dependent manner. More than 95% of Kp was killed when the concentration of GO was at 250.0 μg/mL. After treatment with GO, Kp also showed reduced infectivity to macrophage MH-S cells, thus increased cell viability. More importantly, antibacterial activity of GO was investigated in mouse models. The infectious potency of Kp after peritoneal injection and intranasal instillation was dramatically inhibited by the treatment of GO. The mortality of mice with Kp infection was decreased when GO was used. Meanwhile, the inflammatory responses in the lung, liver, spleen and kidney were also decreased after infected with Kp-GO. Taken together, these findings indicate that GO might be a potential therapeutic agent for Kp, which may also be used to control other MDR bacteria that cause severe disease in clinics. Meanwhile, Kp was still able to cause infection to a certain extent even after the treatment of GO compared with the mocktreated mice, which suggests that the antimicrobial activity of graphene materials at the bacterial level and animal level are not equivalent. Further investigation of antimicrobial activity at the animal level should be considered, which will provide a new critical direction for the application of graphene materials as antimicrobial agents, especially for MDR bacteria. The combination of the traditional antibiotics and antimicrobial nanomaterials in the clinical treatment of infections might be a new strategy to overcome the MDR bacteria.

### **AUTHOR INFORMATION**

# **Corresponding Author:**

\* E-mail addresses: Julia.zhao@und.edu (J.X. Zhao). min.wu@med.und.edu (M. Wu),

### **Present Addresses**

<sup>1</sup>Department of Chemistry, University of North Dakota, Grand Forks, ND 58202, USA.

<sup>2</sup>Department of Biomedical Sciences, School of Medicine and Health Sciences, University of North Dakota, Grand Forks, ND, USA.

<sup>3</sup>Laboratory of Biochemistry and Molecular Biology, School of Life Sciences, Yunnan University, Kunming 650091, China

## ACKNOWLEDGMENT

This work was supported by the North Dakota Department of Commerce grant ND venture phase 1, the National Science Foundation Grants CHE 1709160 to J.X.Z. This work was also supported by the Flight Attendant Medical Research Institute (FAMRI, Grant #103007), National Institute of Health AI109317-01A1, AI101973-01, and AI097532-01A1 to M.W.

We also thank Mr. Ke Xu's valuable suggestions, comments and editing on the manuscript.

### REFERENCES

[1] A. Pompilio, V. Crocetta, M. Scocchi, S. Pomponio, V. Di Vincenzo, M. Mardirossian, et al. Potential novel therapeutic strategies in cystic fibrosis: antimicrobial and anti-biofilm activity of natural and designed alpha-helical peptides against Staphylococcus aureus, Pseudomonas aeruginosa, and Stenotrophomonas maltophilia. BMC. Microbiol. 12 (2012) 145.

- [2] S.P. Lopes, H. Ceri, N.F. Azevedo, M.O. Pereira. Antibiotic resistance of mixed biofilms in cystic fibrosis: impact of emerging microorganisms on treatment of infection. Int. J. Antimicrob. Agents. 40 (2012) 260-263.
- [3] J.-K. Lee, S.-C. Park, K.-S. Hahm, Y. Park. A helix-PXXP-helix peptide with antibacterial activity without cytotoxicity against MDRPA-infected mice. Biomaterials 35 (2014) 1025-1039.
- [4] N. Beyth, I. Yudovin-Farber, R. Bahir, A.J. Domb, E.I. Weiss. Antibacterial activity of dental composites containing quaternary ammonium polyethylenimine nanoparticles against Streptococcus mutans. Biomaterials 27 (2006) 3995-4002.
- [5] M. Guzman, J. Dille, S. Godet. Synthesis and antibacterial activity of silver nanoparticles against gram-positive and gram-negative bacteria. Nanomedicine: NBM. 8 (2012) 37-45.
- [6] H. Wang, J. Liu, X. Wu, Z. Tong, Z. Deng. Tailor-made Au@Ag core-shell nanoparticle 2D arrays on protein-coated graphene oxide with assembly enhanced antibacterial activity. Nanotechnology 24 (2013) 205102.
- [7] J. Chen, H. Peng, X. Wang, F. Shao, Z. Yuan, H. Han. Graphene oxide exhibits broad-spectrum antimicrobial activity against bacterial phytopathogens and fungal conidia by intertwining and membrane perturbation. Nanoscale 6 (2014) 1879-1889.
- [8] S. Chernousova, M. Epple. Silver as antibacterial agent: ion, nanoparticle, and metal. Angew. Chem. Int. Ed. 52 (2013) 1636-1653.
- [9] A. Panáček, L. Kvítek, R. Prucek, M. Kolář, R. Večeřová, N. Pizúrová, et al. Silver colloid nanoparticles: synthesis, characterization, and their antibacterial activity. J. Phys. Chem. B. 110 (2006) 16248-16253.
- [10] Z.-m. Xiu, Q.-b. Zhang, H.L. Puppala, V.L. Colvin, P.J.J. Alvarez. Negligible particle-specific antibacterial activity of silver nanoparticles. Nano Lett. 12 (2012) 4271-4275.

- [11] W. Hu, C. Peng, W. Luo, M. Lv, X. Li, D. Li, et al. Graphene-based antibacterial paper. ACS Nano. 4 (2010) 4317-4323.
- [12] O. Akhavan, E. Ghaderi. Toxicity of graphene and graphene oxide nanowalls against bacteria. ACS Nano. 4 (2010) 5731-5736.
- [13] Y. Tu, M. Lv, P. Xiu, T. Huynh, M. Zhang, M. Castelli, et al. Destructive extraction of phospholipids from Escherichia coli membranes by graphene nanosheets. Nat. Nanotechnol. 8 (2013) 594-601.
- [14] J. He, X. Zhu, Z. Qi, C. Wang, X. Mao, C. Zhu, et al. Killing dental pathogens using antibacterial graphene oxide. ACS Appl. Mater. Interfaces, 7 (2015) 5605–5611.
- [15] M. Khan, H. N. Abdelhamid, H. F. Wu. Near infrared (NIR) laser mediated surface activation of graphene oxide nanoflakes for efficient antibacterial, antifungal and wound healing treatment. Colloids Surf., B 127 (2015) 281-291.
- [16] D.R. Dreyer, S. Park, C.W. Bielawski, R.S. Ruoff. The chemistry of graphene oxide. Chem. Soc. Rev. 39 (2010) 228-240.
- [17] K.S. Novoselov, V.I. Falko, L. Colombo, P.R. Gellert, M.G. Schwab, K. Kim. A roadmap for graphene. Nature 490 (2012) 192-200.
- [18] Fe. Li, H. Pei, L. Wang, J. Lu, J. Gao, B. Jiang, et al. Nanomaterial-based fluorescent DNA analysis: a comparative study of the quenching effects of graphene oxide, carbon nanotubes, and gold nanoparticles. Adv. Funct. Mater. 23(2013) 4140-4148.
- [19] Y. Tu, W. Li, P. Wu, H. Zhang, C. Cai. Fluorescence quenching of graphene oxide integrating with the site-specific cleavage of the endonuclease for sensitive and selective microRNA detection.

  Anal. Chem. 85 (2013) 2536-2542.

- [20] X. Wu, F. Tian, W. Wang, J. Chen, M. Wu, J.X. Zhao. Fabrication of highly fluorescent graphene quantum dots using l-glutamic acid for in vitro/in vivo imaging and sensing. J. Mater. Chem. C. 1 (2013) 4676-4684.
- [21] C. Wang, J. Li, C. Amatore, Y. Chen, H. Jiang, X.-M. Wang. Gold nanoclusters and graphene nanocomposites for drug delivery and imaging of cancer cells. Angew. Chem. Int. Ed. 50 (2011) 11644-11648.
- [22] S. Shi, K. Yang, H. Hong, H.F. Valdovinos, T.R. Nayak, Y. Zhang, et al. Tumor vasculature targeting and imaging in living mice with reduced graphene oxide. Biomaterials 34 (2013) 3002-3009.
- [23] W. Zhang, Z. Guo, D. Huang, Z. Liu, X. Guo, H. Zhong. Synergistic effect of chemophotothermal therapy using PEGylated graphene oxide. Biomaterials 32 (2011) 8555-8561.
- [24] Y. Wang, K. Wang, J. Zhao, X. Liu, J. Bu, X. Yan, et al. Multifunctional mesoporous silicacoated graphene nanosheet used for chemo-photothermal synergistic targeted therapy of glioma. J. Am. Chem. Soc. 135 (2013) 4799-4804.
- [25] Y. Pan, N.G. Sahoo, L. Li. The application of graphene oxide in drug delivery. Expert. Opin. Drug. Deliv. 9 (2012) 1365-1376.
- [26] L. Feng, Z. Liu. Graphene in biomedicine: opportunities and challenges. Nanomedicine 6 (2011) 317-324.
- [27] K. Yang, L. Feng, X. Shi, Z. Liu. Nano-graphene in biomedicine: theranostic applications. Chem. Soc. Rev. 42 (2013) 530-547.
- [28] S. Liu, T.H. Zeng, M. Hofmann, E. Burcombe, J. Wei, R. Jiang, et al. Antibacterial activity of graphite, graphite oxide, graphene oxide, and reduced graphene oxide: membrane and oxidative stress. ACS Nano. 5 (2011) 6971-6980.

- [29] S. Liu, M. Hu, T.H. Zeng, R. Wu, R. Jiang, J. Wei, et al. Lateral dimension-dependent antibacterial activity of graphene oxide sheets. Langmuir 28 (2012) 12364-12372.
- [30] B.Z. Ristic, M.M. Milenkovic, I.R. Dakic, B.M. Todorovic-Markovic, M.S. Milosavljevic, M.D. Budimir, et al. Photodynamic antibacterial effect of graphene quantum dots. Biomaterials 35 (2014) 4428-4435.
- [31] M.C. Wu, A.R. Deokar, J.H. Liao, P.Y. Shih, Y.C. Ling. Graphene-based photothermal agent for rapid and effective killing of bacteria. ACS Nano. 7 (2013) 1281-1290.
- [32] J.D. Mangadlao, C.M. Santos, M.J.L. Felipe, A.C.C de Leon, D.F. Rodrigues, R.C. Advincula. On the antibacterial mechanism of graphene oxide (GO) langmuir-blodgett films. Chem. Commun. 51 (2015) 2886-2889.
- [33] H. E. Karahan, L. Wei, K. Goh, Z. Liu, O. Birer, F. Dehghani, et al. Bacterial physiology is a key modulator of the antibacterial activity of graphene oxide. Nanoscale. 8 (2016) 17181-17189.
- [34] W. Shao, X. Liu, H. Min, G. Dong, Q. Feng, S. Zuo. Preparation, characterization, and antibacterial activity of silver nanoparticle-decorated graphene oxide nanocomposite. ACS Appl. Mater. Interfaces. 7 (2015) 6966-6973.
- [35] X. Li, X. Zhou, Y. Ye, Y. Li, J. Li, B. Privratsky, et al. Lyn regulates inflammatory responses in Klebsiella pneumoniae infection via the p38/NF-kappaB pathway. Eur. J. Immunol. 44 (2014) 763-773.
- [36] Q. Guo, N. Shen, K. Yuan, J. Li, H. Wu, Y. Zeng, et al. Caveolin-1 plays a critical role in host immunity against Klebsiella pneumoniae by regulating STAT5 and Akt activity. Eur. J. Immunol. 42 (2012) 1500-1511.

- [37] S. Kannan, H. Pang, D.C. Foster, Z. Rao, M. Wu. Human 8-oxoguanine DNA glycosylase increases resistance to hyperoxic cytotoxicity in lung epithelial cells and involvement with altered MAPK activity. Cell. Death. Differ.13 (2006) 311-323.
- [38] Y.H. He, M. Wu, M. Kobune, Y. Xu, M.R. Kelley, W.J. Martin, 2nd. Expression of yeast apurinic/apyrimidinic endonuclease (APN1) protects lung epithelial cells from bleomycin toxicity. Am. J. Respir. Cell. Mol. Biol. 25 (2001) 692-698.
- [39] K. Yuan, C. Huang, J. Fox, D. Laturnus, E. Carlson, B. Zhang, et al. Autophagy plays an essential role in the clearance of Pseudomonas aeruginosa by alveolar macrophages. J. Cell. Sci. 125 (2012) 507-515.
- [40] Y.H. He, Y. Xu, M. Kobune, M. Wu, M.R. Kelley, W.J. Martin, 2nd. Escherichia coli FPG and human OGG1 reduce DNA damage and cytotoxicity by BCNU in human lung cells. Am. J. Physiol. Lung. Cell. Mol. Physiol. 282 (2002) L50-55.
- [41] G. Li, K. Yuan, C. Yan, J. Fox Iii, M. Gaid, W. Breitwieser, et al. 8-Oxoguanine-DNA glycosylase 1 deficiency modifies allergic airway inflammation by regulating STAT6 and IL-4 in cells and in mice. Free. Radic. Biol. Med. 52 (2012) 392-401.

# Figures

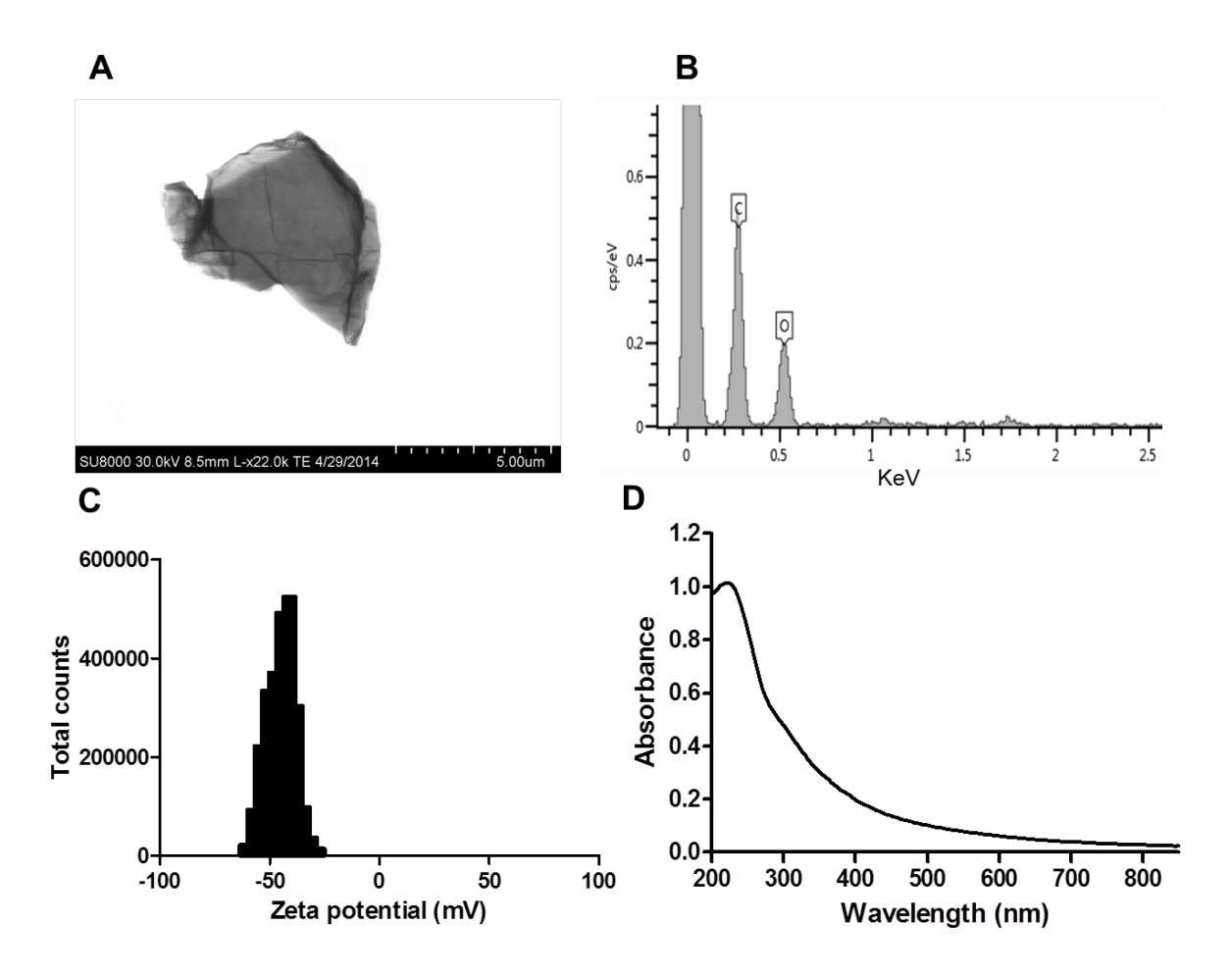


**Figure 1.** Characterization of GO using different methodology. (A) STEM image. (B) EDS pattern. (C) zeta potential. (D) UV-vis spectrum.

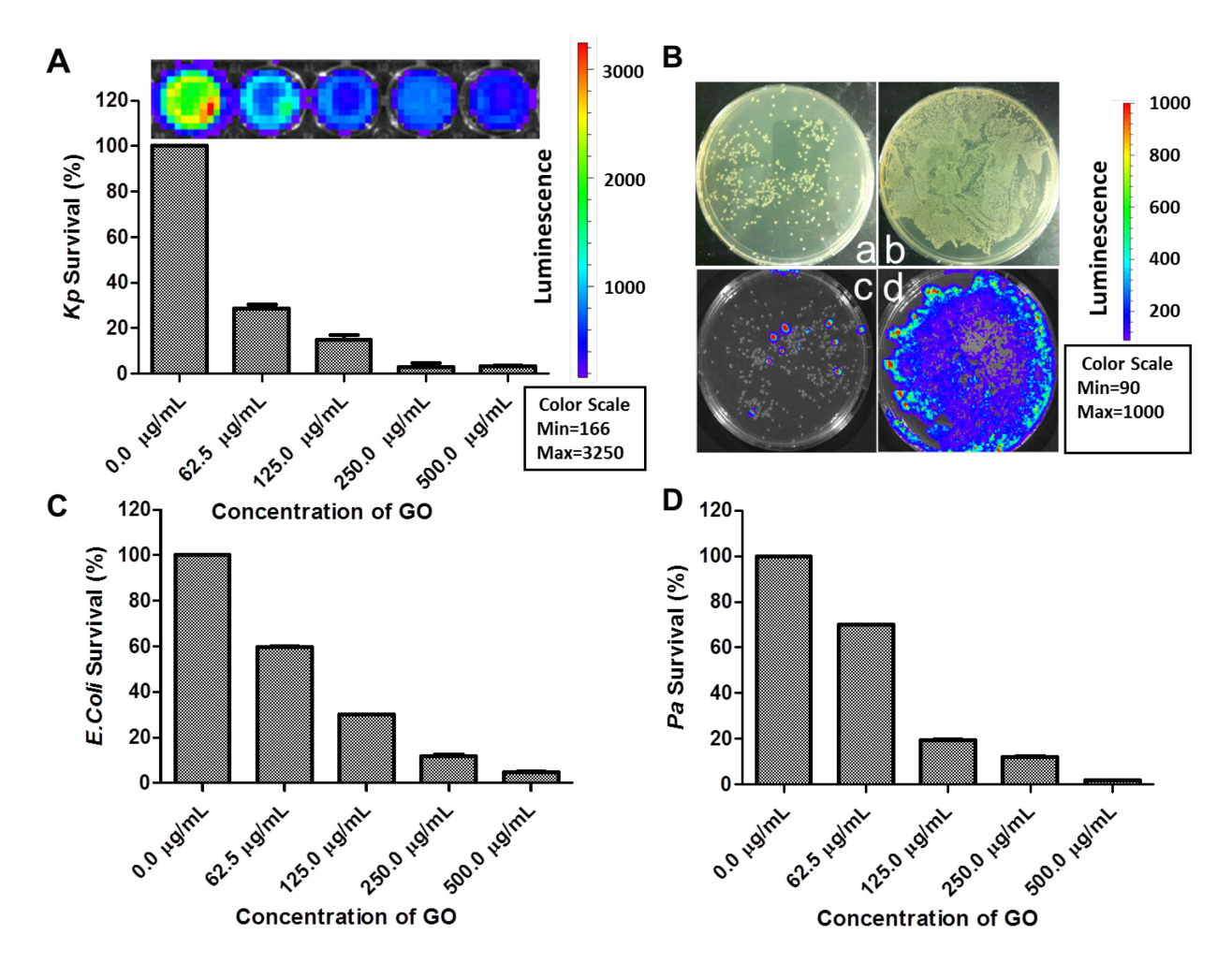


**Figure 2.** Concentration-dependent antibacterial property of GO. (A) *Kp* survival rate after treatment with different concentrations of GO. Inset: Bioluminescence images of *Kp* bacteria after incubation with different concentrations of GO. From left to right: 0, 62.5, 125.0, 250.0, and 500.0 μg/mL of GO. (B) Representative photographs (a and b) and bioluminescence images (c and d) of *Kp* bacterial colonies treated with 250.0 μg/mL of GO (a and c) and without GO (b and d) formed on LB-agar plates. (C) The *E. coli* survival rate after treatment with different concentrations of GO. (D) *Pa* survival rate after treatment with different concentrations of GO. The survival rate was calculated by measuring the OD600.

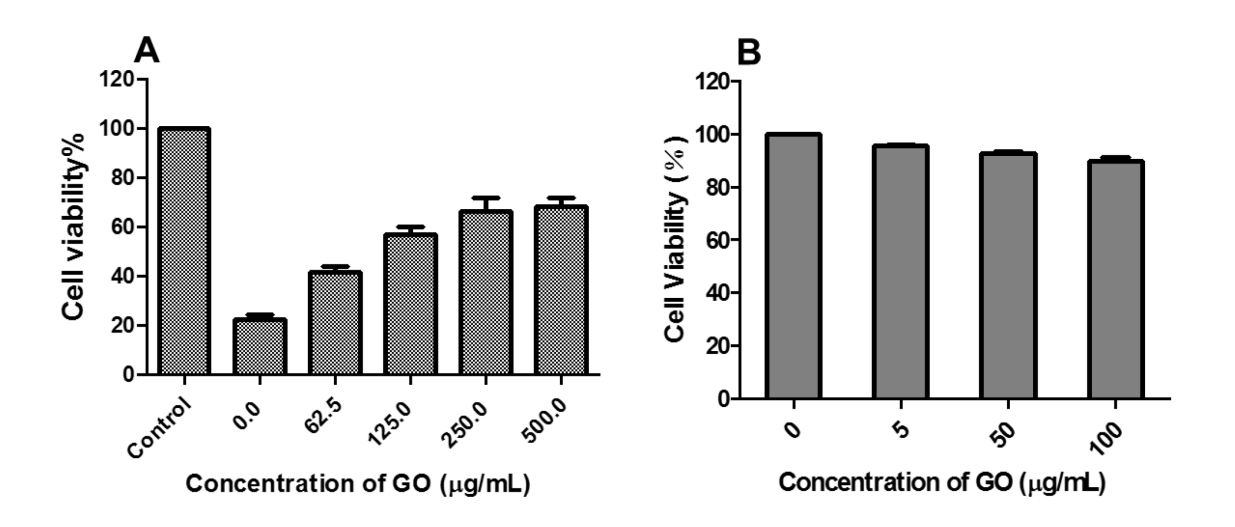


**Figure 3. (A)** Relative viability of MH-S cells infected by GO treated Kp (Kp-GO). (B) Macrophage cell viability without Kp at different concentrations of GO.

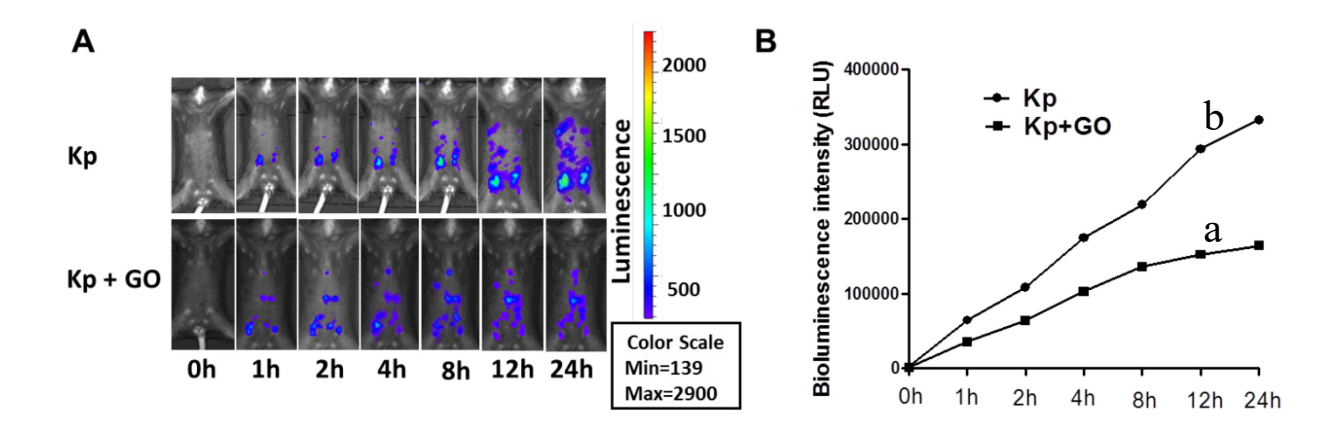


**Figure 4.** GO decreased Kp infection severity in mice. (A) Bioluminescence images of mice at different time period after intraperitoneal injection of untreated Kp bacteria (top) and GO-treated Kp (bottom). (B) Semiquantitive bioluminescence intensity of mice after the infection of GO-treated Kp (curve a) and untreated Kp (curve b).

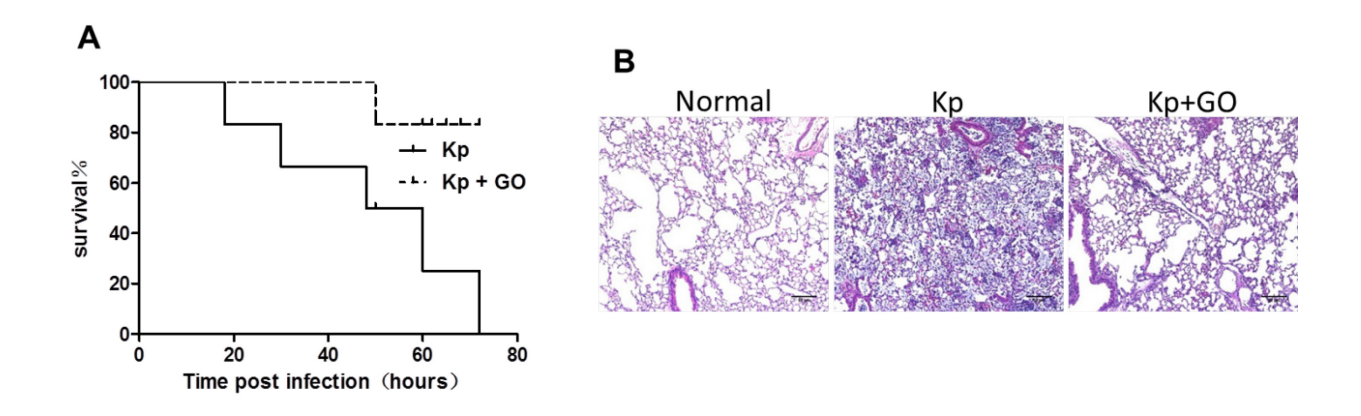
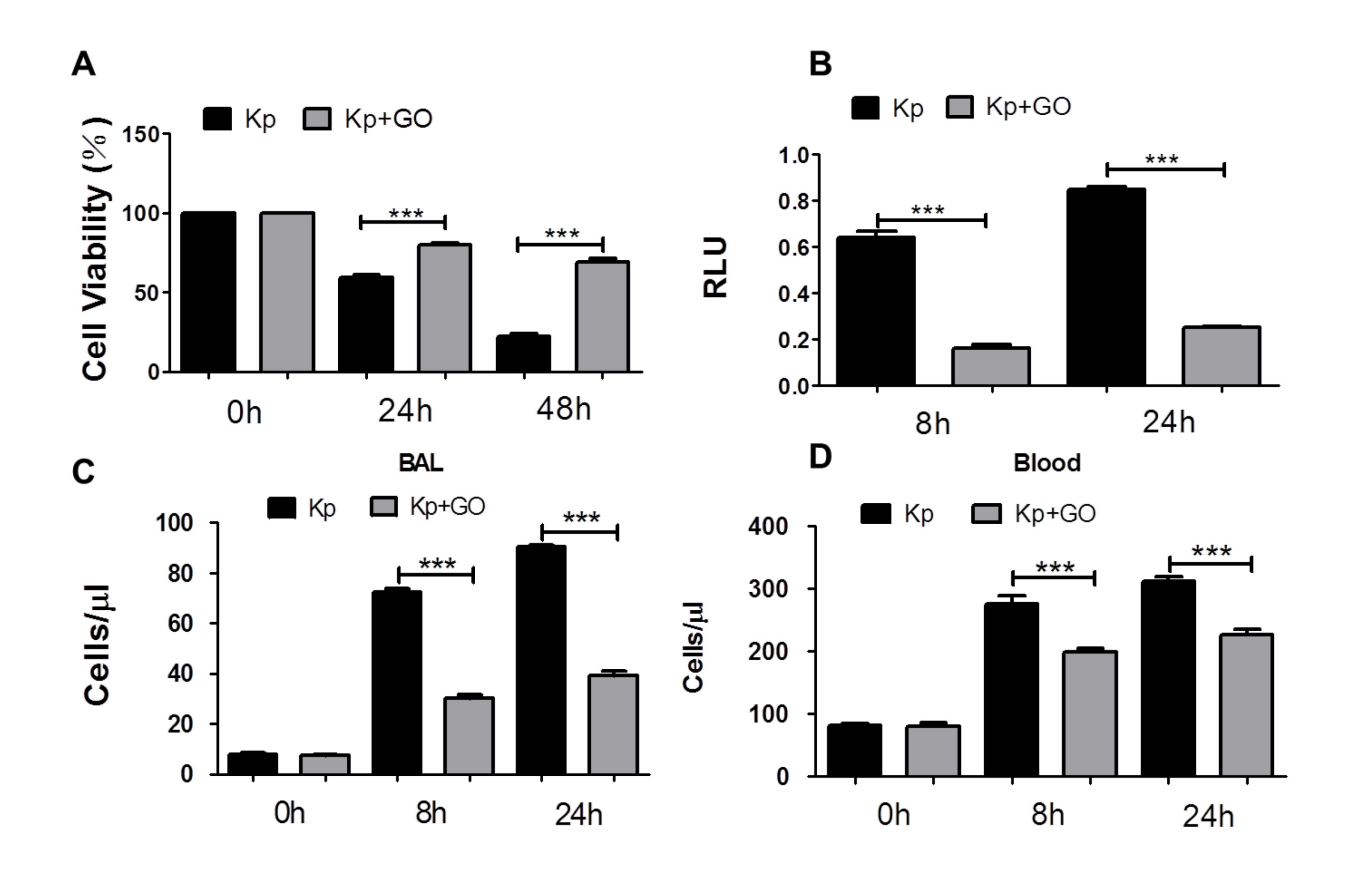
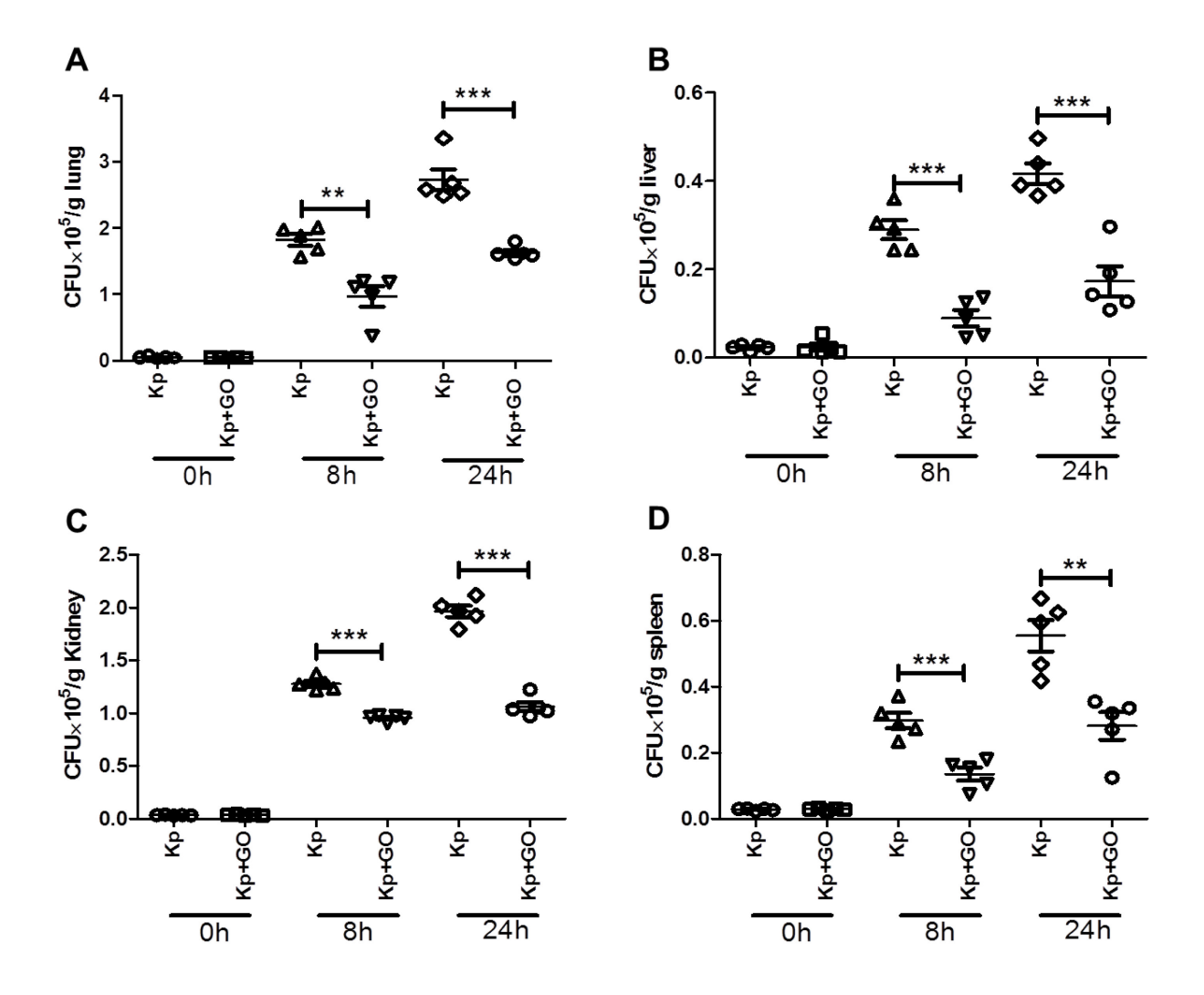


Figure 5. GO decreased mortality rates and tissue damage in mice after infected by Kp. (A) Kaplan-Meier survival curves were obtained by infecting mice with GO-treated Kp (curve a) and untreated Kp (curve b), respectively (n=5). (B) Morphological evidence of lung injury and inflammatory responses as assessed by H & E staining histological analysis (20×, scale bar = 50  $\mu$ m). Left: normal lung tissue without bacterial infection; Middle: untreated Kp infected lung tissue; Right: lung tissue with GO treated Kp infection.



**Figure 6.** (A) Cell viability of AM after bacterial infection by MTT assay. (B) ROS production in AM cells detected using an NBT assay. (C and D) PMN infiltration in the BAL and blood was counted by HEMA staining (Thermofisher). \*\*\*p < 0.001; RLU: relative LUC units.



**Figure 7.** The lung (A), liver (B), spleen (C), and kidneys (D) showed significantly decreased bacterial burdens in GO-Kp infected mice (Mann Whitney U test). \*\*p < 0.01; \*\*\*p < 0.001.

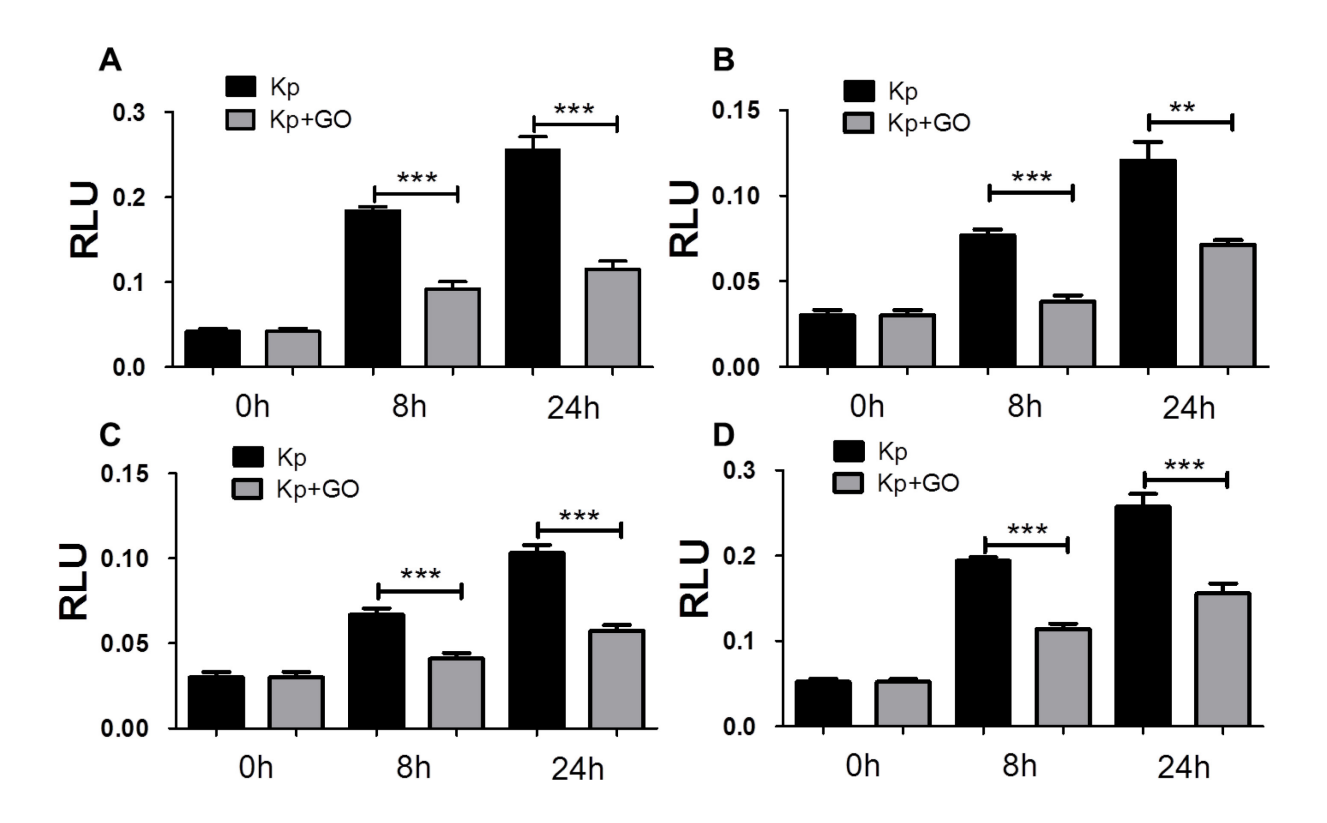


**Figure 8.** Decreased MPO activity in the lung (A), liver (B), spleen (C), and kidneys (D) of GO-Kp treated mice at 8 h and 24 h. (n = 3) Data are shown as mean + SE of mice per group and are representative of three independent experiments. \*\*p < 0.01; \*\*\*p < 0.001; one-way ANOVA (Tukey's post hoc). RLU: relative LUC units.